PII S0301-5629(98)00123-9

C *Original Contribution*

VIBRATION SONOELASTOGRAPHY AND THE DETECTABILITY OF LESIONS

KEVIN J. PARKER,* DONGSHAN FU,* SHERYL M. GRACESWKI,† FAI YEUNG,* and STEPHEN F. LEVINSON*‡

Departments of *Electrical and Computer Engineering, †Mechanical Engineering, and ‡Physical Medicine and Rehabilitation, University of Rochester, Rochester, NY 14627 USA

(*Received* 16 *March* 1998; *in final form* 16 *July* 1998)

Abstract—Vibration sonoelastography has been developed for the detection of hard lesions in relatively soft tissue. The basic concept is to propagate low-amplitude and low-frequency shear waves (with displacements below 0.1 mm and frequencies typically below 1000 Hz) through deep organs, and displaying the vibration response in real-time using advanced color Doppler imaging techniques. A hard inhomogeneity, such as a tumor, will produce a localized disturbance in the vibration pattern, forming the basis for detection even when the tumor is isoechoic on B-scan images. This paper focuses on the important quantitative issues concerning the detectability or inherent contrast of lesions. The specific factors of lesion size, relative stiffness and vibration frequency are studied using theoretical models, finite element methods and experimental measurements on tissue-mimicking materials. The results indicate that detectability increases with vibration (shear wave) frequency; however, loss mechanisms ultimately limit the penetration of higher vibration frequencies (in the kHz range).

Key Words: **Sonoelasticity, Sonoelastography, Ultrasound, Doppler, Shear waves, Vibration, Tumor detection, Tissue viscoelastic properties.**

INTRODUCTION

Vibration sonoelasticity imaging has been proposed for detection of hard lesions (Lerner et al. 1988, 1990; Parker et al. 1990; Yamakoshi et al. 1990; Gao et al. 1995, 1997) and also for the study of tissue viscoelastic properties (Levinson et al. 1995). In these methods, the amplitude and/or phase of vibration of the tissue is estimated and displayed using ultrasound pulse echo techniques specially designed for the Doppler signal of vibrating targets (Huang et al. 1990, 1992; Yamakoshi et al. 1990).

Other independent work has centered on estimating tissue properties using incremental compression of tissues (Ophir et al. 1991; O'Donnell et al. 1994; Skovoroda et al. 1994). The literature in this field has been reviewed in recent articles (Gao et al. 1996; Ophir et al. 1997), and is rapidly growing. Extensions to other modalities and many anatomical structures, such as the eye, are described in one review (Gao et al. 1996).

A theoretical framework has been established for the detection of inhomogeneities in a vibrating medium (Gao et al. 1995, 1997) with application to the liver, the prostate and other organs. Here, this framework will be extended to include a detailed treatment of lesion detectability. This paper examines theoretical relationships, along with new finite element models and experiments using tissue-mimicking materials, to establish the funda-

THEORY

For a linear viscoelastic and isotropic 3-D structure, solutions for the wave motion cannot be obtained analytically, except for the simplest geometry and boundary conditions. These problems are often made tractable by incorporating some assumptions and simplifications. Gao et al. (1995) have formulated a mathematical model for vibration amplitude sonoelastography. A lesion is modeled as an elastic inhomogeneity inside a lossy homogeneous elastic medium. The homogeneous medium has constant stiffness E_0, and the small inhomogeneity has stiffness $E = E_0 + \Delta E$. The vibration patterns of the medium, with and without the inhomogeneity, are derived from the vector displacement equations.

The wave motion equation can be expressed in term of the displacements as:

$$\frac{E}{2(1+\nu)(1-2\nu)}\nabla\nabla\cdot\bar{u} + \frac{E}{2(1+\nu)}\nabla^2\bar{u} = \rho\frac{\partial^2\bar{u}}{\partial t^2}, \tag{1}$$

where E, ν, ρ and $\bar{u}$ are the Young's modulus, Poisson's ratio, mass density and displacement vector, respectively. The above motion equation can be decomposed into two decoupled motion equations, one governing longitudinal wave motion, and the other governing shear wave motion. Only the shear wave equation is chosen for consideration, for the following reasons. First, the longitudinal waves have wavelengths much larger than organs of interest at the frequencies used in sonoelastography (Parker et al. 1992). In addition, biological tissue is nearly incompressible, so the Poisson's ratio approaches 0.5 (Fung 1981; Parker et al. 1990). At this Poisson's ratio, the wave dilatation that represents the longitudinal wave motion is close to zero; thus, the shear wave motion $\bar{u}_T$ dominates the wave propagation. In a homogeneous medium, the shear wave component is governed by the wave equation (Gao et al. 1995):

$$\frac{E}{2(1+\nu)}\nabla^2\bar{u}_T = \rho\frac{\partial^2\bar{u}_T}{\partial t^2}. \tag{2}$$

The shear wave eqn (2) for the medium with inhomogeneity is expressed as:

$$\nabla^2\bar{u}_T - \frac{1}{C_0^2(1+\gamma)}\frac{\partial^2\bar{u}_T}{\partial t^2} = 0, \tag{3}$$

where

$$C_0 = \left[\frac{E_0}{2\rho(1+\nu)}\right]^{1/2}, \tag{4}$$

and

$$\gamma = \frac{E - E_0}{E_0}. \tag{5}$$

E_0 is Young's modulus of the homogeneous background material where $\gamma = 0$. E is Young's modulus of the inhomogeneous material where $\gamma \neq 0$. $\gamma > 0$ indicates a hard lesion and $\gamma < 0$ indicates a soft lesion. Biological tissue is lossy and typically modeled as a viscoelastic material (Fung 1981). Therefore, a relaxation term should be included in eqn (3) (Kinsler et al. 1982). Assuming that the external vibration has a harmonic time dependence $\bar{u}_T = \bar{U}\exp(i\omega t)$, eqn (3) with a loss term becomes:

$$\nabla^2\bar{U} + \frac{K^2}{(1+\gamma)}\bar{U} - \frac{iK^2}{Q_0(1+\gamma)}\bar{U} = 0, \tag{6}$$

where $K = \omega/C_0$ and Q_0 is the Q factor of the system at the frequency ω.

There is no closed form solution to eqn (6). To gain insight into the effect of the inhomogeneity on the wave fields, the "elastic-Born" approximation is used to rear-

shown in Fig. 1. Note the leveling off of b as $E/E_0 \to \infty$; that is, as the inhomogeneity becomes extremely stiff. However, the assumptions involved in deriving the "elastic-Born" equation limit the range of applicability of the equations to some limited range of E/E_0 near unity. Gao

Fig. 3. Relative displacement amplitude d/d_0 vs. relative lesion stiffness E/E_0 from the FEM study ($+-60$ Hz, circle = 100 Hz; diamond = 300 Hz; square = 400 Hz). The lesion size is 6 mm × 6 mm. Note that the general trend follows the theoretical derivation of the b term as shown in Fig. 1.

field, even at the lesion boundaries, although the lesion and the background material have different elasticities. Therefore, the vibration amplitude imaging technique is not suitable for small lesion detection at very low frequencies (below 200 Hz). Instead, strain imaging may be useful in this case. Given the external forces, the strain is proportional to the material elasticity because the stress is continuous at the boundary between the lesion and the homogeneous medium. Thus, the strain in the lesion region differs from that in the background media. Figure 6 compares the strain images for a homogeneous and inhomogeneous ($E/E_0 = 5$) medium at 100 Hz, where the brightness is proportional to the vertical strain component. At this low frequency, the lesion in the strain image is much more evident than that in the displacement amplitude image in Fig. 5a. However, because strain estimations require derivative operators, the strain image will be sensitive to noise. Although the strain image is promising, this paper concentrates on the displacement image technique.

Fig. 4. Grey-scale images of the vertical displacement amplitudes at 400 Hz vibration. Each image is 40 mm width by 40 mm height, and is a region of interest within the domain shown in Fig. 2. The lesion size is 6 mm × 6 mm. (left) Soft lesion $E/E_0 = 0.2$; middle = no lesion; right = hard lesion $E/E_0 = 5$.

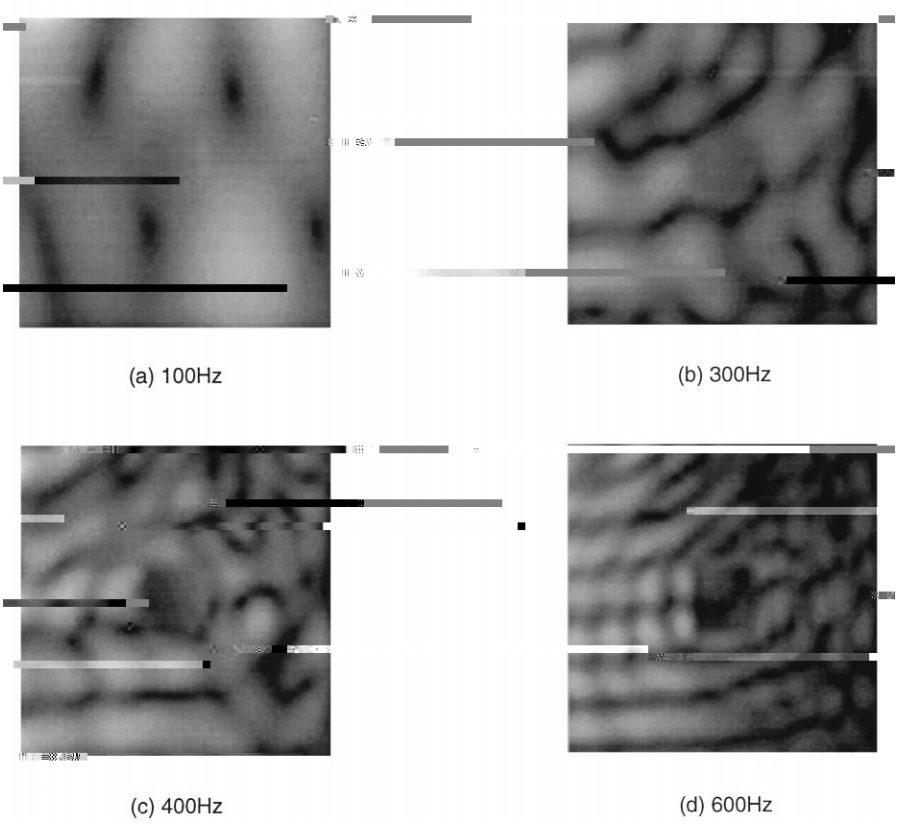

Fig. 5. Grey-scale images of the vertical displacement amplitudes for $E/E_0 =$

So far, only the amplitude of the vibration motion field has been considered. The phase may also be useful in determining the viscoelastic properties of a material (Yamakoshi et al. 1990; Levinson et al. 1995). The phase color maps at 600 Hz for the homogeneous and for the hard lesion $E/E_0 = 5$ are sketched in Fig. 7. It is a visual representation of spatial changes of phase of the vibration motion field. The color model of intensity, hue and saturation (HIS) is converted to RGB color model. Here, both the intensity and saturation are set to 1, and the hue

represents the phase, which has a range from 0 to 360°. The lesion can be identified in the center of the static image of Fig. 7, but is much more clearly visualized in the animation of a phase color-map sequence.

The detectability of a lesion also depends on its size or volume. Figure 8 shows how the detectability depends on lesion size for an excitation frequency of 400 Hz. The detectability increases dramatically when the lesion size increases. The grey-scale vibration images for different lesion sizes are displayed in Fig. 9 for the case $E/E_0 = 5$. The lesion size is (left) 4 mm $\times$ 4 mm; (middle) 6 mm $\times$ 6 mm; and (right) 8 mm $\times$ 8 mm. A large lesion causes a large disturbance region, so the lesion visibility is better. A small lesion with size 4 mm $\times$ 4 mm is thought to be detectable because the darker lesion region in the image can be identified.

The exact amount of loss and its frequency-dependence in tissue at these frequencies is unknown. However, we can predict the effect of damping by numerical simulation. Figure 10 shows that the lesion detectability decreases with increasing damping ratio. For a purely elastic case, the average lesion displacement is 80% below the corresponding average displacement in a homogeneous medium. Even for a small damping ratio

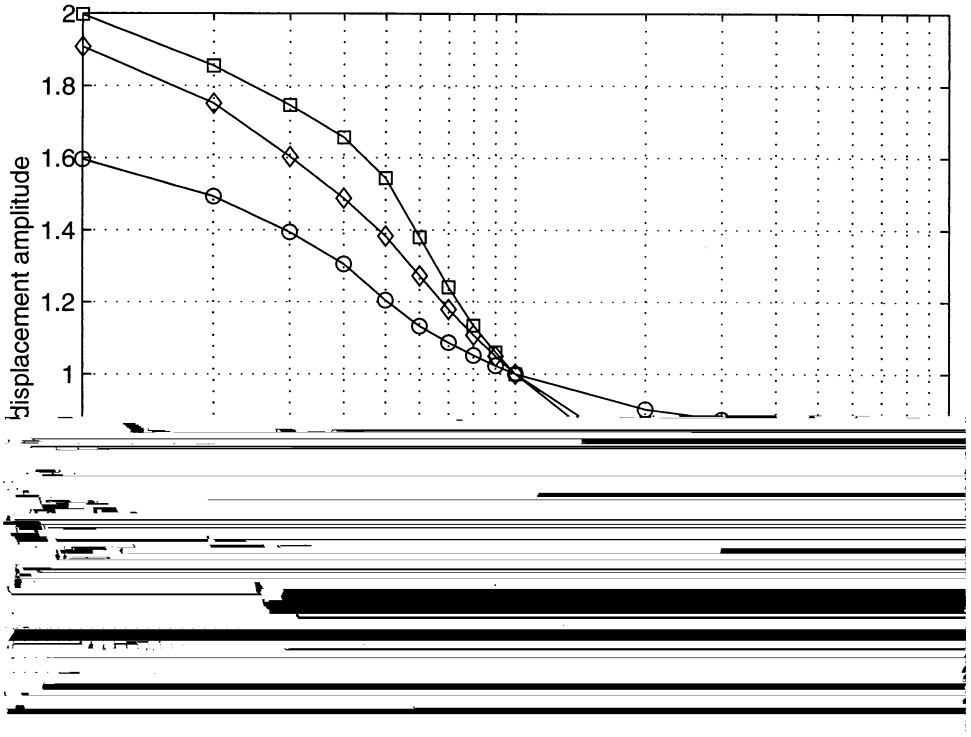

Fig. 8. Relative displacement amplitude d/d_0 vs. relative lesion stiffness E/E_0 at vibration frequency 400 Hz for different size lesions: circle = 4 mm × 4 mm; diamond = 6 mm × 6 mm; square = 8 mm × 8 mm.

the lesion is 7 times that of the homogeneous material of the phantom. The model is adaptively meshed with approximately 15,000 3-D hexahedral isoparametric elements, where the mesh is finer in the region close to the lesion and coarser elsewhere. The lesion is meshed by 16 elements. The FEM mesh model provides adequate resolution over the vibration frequency range of interest.

The grey-scale images obtained from the simulation data in the region of interest are shown in Fig. 12a and b for 248 Hz and 318 Hz, respectively. The cubic spline interpolation is performed on the FEM data before displaying the image, so that the images have higher spatial sampling. The shape of the phantom and the boundary conditions are complicated, so the vibration pattern is not simple. However, the lesion regions are readily located. The images will be compared with the experimental results.

EXPERIMENTAL RESULTS

The tissue-mimicking phantom in our experiments was manufactured by Computerized Imaging Reference

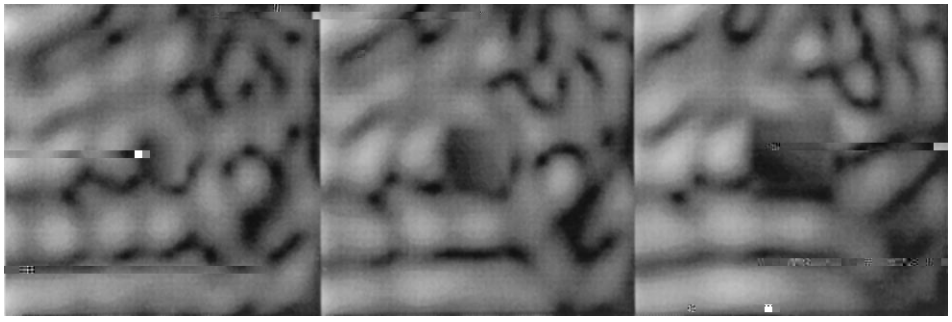

Fig. 9. Grey-scale images of the vertical displacement amplitudes at a vibrationsqu64(imawtr)-4443 0 diffons:ima8G(sRplaceme U75g

The small strain range was chosen so that the basic linear elastic equations were satisfied. The viscosity cannot be obtained from the static measurement. Both elasticity and viscosity were measured using a sensitive dynamic measurement instrument (Solids Analyzer RSA-II). Be-

theory. The systematic and quantitative 2-D results showed that detectability increases with lesion stiffness and size. For the cases considered, detectability increased with the vibration frequency in a certain range. However, the damping mechanism ultimately limits the penetration of high-vibration frequencies. Small lesions are not easily detected at very low frequencies (below 200 Hz) using the vibration-amplitude imaging technique. Instead, the strain imaging technique may be used for lesion detection at very low-frequency vibration. A tissue-mimicking phantom was numerically simulated with the 3-D FEM model. The experiments were performed on the phantom using advanced Doppler imaging techniques. The experimental results corresponded well with the predictions of the 3-D FEM simulations. The results presented in this paper provide guidelines for clinical application of vibration sonoelastography or for any coherent imaging system capable of measuring vibration within tissue.

Acknowledgements—This work was supported in part by the NSF/NYS center for electronic imaging system, and by NIH. The loan of equipment from GE Medical Systems is gratefully acknowledged. The authors especially thank Drs. Kai Thomenius and Anne Hall of GE for